Non-Gaussianity and coherent vortex simulation for two-dimensional turbulence using an adaptive orthogonal wavelet basis

Marie Farge
Laboratoire de Météorologie Dynamique du CNRS, Ecole Normale Supérieure de Paris, 24 rue Lhomond, 75231 Paris Cedex 05, France
and Centre de Mathématiques et Leurs Applications, Ecole Normale Supérieure de Cachan, 61 Avenue du Président Wilson, 94235 Cachan Cedex, France

Kai Schneider
Institut für Chemische Technik, Universität Karlsruhe (TH), Kaiserstrasse 12, 76128 Karlsruhe, Germany

Nicholas Kevlahan
Department of Mathematics and Statistics, McMaster University, Hamilton, Ontario L8S 4K1, Canada
and Centre de Mathématiques et Leurs Applications, Ecole Normale Supérieure de Cachan, 61 Avenue du Président Wilson, 94235 Cachan Cedex, France

We decompose turbulent flows into two orthogonal parts: a coherent, inhomogeneous, non-Gaussian component and an incoherent, homogeneous, Gaussian component. The two components have different probability distributions and different correlations, hence different scaling laws. This separation into coherent vortices and incoherent background flow is done for each flow realization before averaging the results and calculating the next time step. To perform this decomposition we have developed a nonlinear scheme based on an objective threshold defined in terms of the wavelet coefficients of the vorticity. Results illustrate the efficiency of this coherent vortex extraction algorithm. As an example we show that in a 256^2 computation 0.7% of the modes correspond to the coherent vortices responsible for 99.2% of the energy and 94% of the enstrophy. We also present a detailed analysis of the nonlinear term, split into coherent and incoherent components, and compare it with the classical separation, e.g., used for large eddy simulation, into large scale and small scale components. We then propose a new method, called coherent vortex simulation (CVS), designed to compute and model two-dimensional turbulent flows using the previous wavelet decomposition at each time step. This method combines both deterministic and statistical approaches: (i) Since the coherent vortices are out of statistical equilibrium, they are computed deterministically in a wavelet basis which is remapped at each time step in order to follow their nonlinear motions. (ii) Since the incoherent background flow is homogeneous and in statistical equilibrium, the classical theory of homogeneous turbulence is valid there and we model statistically the effect of the incoherent background on the coherent vortices. To illustrate the CVS method we apply it to compute a two-dimensional turbulent mixing layer. © *1999 American Institute of Physics.*
[S1070-6631(99)04608-5]

I. INTRODUCTION

In this article we introduce a new approach for computing turbulence which is based on the observation that turbulent flows contain both an organized part (the coherent vortices) and a random part (the incoherent background flow). The direct computation of fully developed turbulent flows involves such a large number of degrees of freedom that it is out of reach for the present and near future. Therefore some statistical modeling is needed to drastically reduce the computational cost. The problem is difficult because the statistical structure of turbulence is not Gaussian, although most statistical models assume simple Gaussian statistics. The approach we propose is to split the problem in two: (i) the determinist computation of the non-Gaussian components of the flow and (ii) the statistical modeling of the Gaussian components (which can be done easily since they are completely characterized by their mean and variance). We

present a wavelet-based method which performs such a separation. The non-Gaussianity of turbulent fields results from the nonlinear dynamics of Navier–Stokes equations, which produces strong gradients and organized vortices. We then check *a posteriori* that the non-Gaussian components actually correspond to the coherent vortices.

Of course this approach is only of interest if the Gaussian part (to be modeled) is responsible for the vast majority of degrees of freedom and if the coherent vortex part (to be computed) contains a small number of degrees of freedom which are responsible for most of the nonlinear term (and hence the cascade). We have found this to be the case when we apply our method to two-dimensional turbulence. Note that, although we apply our method in two dimensions, it can also be applied to three-dimensional flows. In fact, the dynamics of two- and three-dimensional turbulence may not be as different as is usually assumed, since in two dimensions

2187

vorticity gradient stretching and palinstrophy production plays a dynamical role similar to that of vortex stretching and enstrophy production in three dimensions. Moreover Biot–Savart's law, Kelvin's theorem, and Helmholtz's theorem are valid regardless of the dimension, and they form the basis of our computational scheme, which is written using the vorticity–velocity formulation of the Navier–Stokes equations.

Coherent vortices are localized concentrations of vorticity, tending to vortex spots in two dimensions and to vortex tubes in three dimensions. They are produced by the nonlinear dynamics of incompressible Navier–Stokes equations. The main difference between two and three dimensions is that vortices are much more stable in two dimensions due to the lack of vortex stretching. The velocity associated with a coherent vortex is less local than the vorticity, because of the Biot–Savart kernel. Therefore, as soon as coherent vortices are present in turbulent flows, one achieves higher compression by filtering the vorticity field rather than the velocity field, since the vorticity field is more intermittent and hence better suited for adaptive computation. This motivates the choice of the vorticity–velocity formulation of Navier–Stokes equations instead of the velocity–pressure formulation.

In the case of two-dimensional flows, we have shown[1] that the strain imposed by the coherent vortices on the background flow inhibits the development of nonlinear instabilities and the formation of new vortices in the background. This led us to conjecture that, for large Reynolds number flows, the density of coherent vortices should be roughly constant (and is probably quite small). If this conjecture is verified, it will guarantee that the number of resolved modes of our method will remain bounded for any Reynolds number. However, this inhibition is not present if coherent vortices have not yet formed, which is the case in wall regions for bounded flows, or during the early evolution of unbounded flows initialized with random conditions.

In this paper we propose a new way of computing and modeling turbulence, called coherent vortex simulation (CVS), which is based on the conjecture that coherent vortices are generic in incompressible turbulent flows, in two and three dimensions. It assumes that only the degrees of freedom attached to the coherent vortices are deterministically active and need to be computed exactly. In two dimensions vortices correspond to the elliptical regions of the flow where rotation dominates strain and thus are not well mixed. They experience strain and mixing only during close encounters with other vortices, which results in vorticity filament emission and vortex merging or tearing. However, these events are too rare to allow the coherent vortices to reach a statistical equilibrium state, and thus the central limit theorem does not apply so that meaningful averages cannot be defined. Therefore, one is forced to compute their evolution as exactly as possible, in particular their shape and position. On the other hand, we suppose that all remaining degrees of freedom have reached a quasi-equilibrium state and therefore can be modeled statistically, because they are attached to the well-mixed background flow, which corresponds to hyperbolic regions where strain dominates rotation. Their averages

are well defined, thanks to the central limit theorem which remains valid as long as the coherent vortex strain inhibits any nonlinear instability from developing in the incoherent background flow.[1]

If one can guarantee that the background flow has a Gaussian probability density function (PDF), its total statistical effect can be calculated from its mean and variance. All remaining components exhibit a non-Gaussian PDF and we check that they do indeed correspond to the coherent vortices. In fact, we propose to define the incoherent background flow as those components associated with a Gaussian PDF, and the coherent vortices as all other remaining components.

The paper is organized as follows. In Sec. II we briefly recall the essential features of wavelets and describe the algorithm used to separate the Gaussian (incoherent background) and non-Gaussian (coherent vortex) parts of the flow. We propose a new wavelet-based method to compute turbulent flows (the coherent vortex simulation method), which is presented in Sec. III. The results are discussed in Sec. IV and the paper ends with some conclusions in Sec. V.

II. COHERENT VORTEX EXTRACTION BASED ON THEIR NON-GAUSSIANITY

A. Wavelet representation to study turbulent flows

Inspired by the work of Grossmann and Morlet,[2] we have proposed using wavelets to study turbulent flows.[3,4] Wavelets are functions which are well localized in both physical and spectral space. In addition, their smoothness (which determines the number of times they can be differentiated) and their number of vanishing moments (which determines the number of times they can be integrated) can be controlled. They can efficiently represent data which is neither completely particle-like nor wave-like (e.g., multiscale localized structures). Furthermore, fast wavelet algorithms exist and wavelet bases are available for von Neumann or Dirichlet boundary conditions.[5] The characteristics mentioned above mean that wavelets are suitable for detecting and analyzing the coherent vortices that emerge out of random Gaussian initial conditions, or are created in boundary layers.

The shape of these vortices results from a competition between the Biot–Savart kernel (used to compute to the nonlinear advection term of the Navier–Stokes equation) and the heat kernel (used to compute the linear dissipation term). If one considers initially a Gaussian random field, then the Biot–Savart kernel selects the strongest local maxima (namely the tails of the vorticity PDF which correspond to the strongest singularities, in the sense of Hölder[9]) and locally organizes the flow into vortices whose centers correspond to these initial local maxima. As a result, there are also small scales in the vortex cores, which we have shown using two-dimensional continuous wavelet analyses of two-dimensional[3,4] and three-dimensional[6] turbulent flows. Consequently the coherent vortices are multiscale structures, which are excited all along the inertial range (i.e., from the integral to the dissipative scales).

The Biot–Savart kernel is an integral operator (with $1/r$ decay in dimension two). It is therefore global in physical

space and couples all coefficients of a collocation (i.e., grid-point) projection of the fields. Using a wavelet representation this operator becomes increasingly localized at small scale, due to the vanishing moments of the wavelet. The nonlinear term of the Navier–Stokes equations (3) is optimally localized in a grid-point projection, because the collocation projection commutes with the nonlinear operator. On the contrary, the nonlinear term is delocalized in a Fourier projection where it becomes a convolution. It has been shown[7] that using wavelets one recovers the locality of the nonlinear operator at small scales. Meneveau[8] has studied the dynamics in space and scale of three-dimensional turbulent flows, and the associated energy transfers, by projecting the Navier–Stokes equations onto an orthogonal wavelet basis.

B. Classical vortex extraction methods

One needs a method to extract coherent vortices out of turbulent flows, in order to compute their circulation, spatial support, vorticity and velocity PDFs, and study their dynamics. However, at present there is no consensus on the precise definition of a coherent vortex. The only definition which seems objective is a locally metastable state. In two dimensions a coherent vortex can be unambiguously characterized by a functional relation between the vorticity ω and the streamfunction Ψ in the form $\omega = F(\Psi)$, where F is called the coherence function.[9] One technique to extract coherent vortices from two-dimensional turbulent flows would thus be to plot the pointwise scatter plot of ω versus Ψ and extract the branches which can be fitted by some function F. The points belonging to these branches would correspond to locations where the vorticity field $\omega_>$ is coherent, while the scattered points which do not belong to any branch would correspond to locations in the incoherent background flow $\omega_<$. In practice this method is not feasible because it requires that the computation of F be performed in a frame of reference moving with each coherent vortex.

Other techniques to extract coherent vortices are less objective than the one described above because they depend on a threshold value which has to be defined *a priori*. The simplest method is to choose a vorticity threshold, for instance $\epsilon_C = Z^{1/2}$ with enstrophy $Z = \frac{1}{2}\int \omega^2 \, dx$, and retain as coherent the regions where $|\omega| > \epsilon_C$, while the remainder forms the background flow. The drawback of this clipping method is that it does not preserve the smoothness of ω, and both incoherent and coherent fields will contain spurious discontinuities which will affect their time evolution and their energy spectrum. To avoid this problem we suggest replacing the grid-point representation by a wavelet representation, which does not introduce discontinuities and therefore preserves the spectral properties of the flow when we truncate in this wavelet basis.

Since the wavelet transform is invertible, it is always possible to select a subset of the coefficients and reconstruct a filtered version of the field from them. Using this property, we have proposed[10] using the continuous wavelet representation to extract coherent vortices by discarding all wavelet coefficients outside the influence cones (i.e., the spatial support of the wavelets) attached to the local maxima of the

vorticity field which correspond to the centers of coherent structures.

We have also tried[11,12] to use orthonormal bases made of either wavelets, wavelet packets, or adaptive local cosines (Malvar wavelets) to separate coherent vortices from background flow. We showed that the local cosine representation does not compress the enstrophy as well as wavelets or wavelet packets. First, it smoothes the coherent structures and therefore loses enstrophy, and second, it introduces spurious oscillations in the background, due to the loss of the phase information attached to the weak coefficients. These drawbacks are shared by any Fourier or windowed Fourier representation, because each Fourier component contains nonlocal information and we need the phase information of all Fourier components to reconstruct precisely a given region of the field. Therefore no Fourier technique can properly extract coherent vortices, because as the vorticity field is compressed the coherent vortices disappear and become increasingly mixed with the background flow.[11,12] This is why we prefer to use wavelet or wavelet packet bases.

C. A new wavelet-based vortex extraction method

In this paper we propose a new procedure to extract coherent vortices which uses the projection of the vorticity onto an orthonormal wavelet basis. This extraction scheme is based on the assumption that coherent vortices are responsible for the non-Gaussianity of the PDF of vorticity. Therefore it is designed such that the discarded vorticity coefficients have a Gaussian PDF. This is the only *a priori* assumption we make, apart from the choice of the wavelet basis. Note that we do not assume any shape or intensity of the vortices. The coherent vortices correspond to all modes remaining after discarding those with a Gaussian PDF. In other words, we define the coherent vortices to be the non-Gaussian part of the vorticity field. Although the method is verified here only for a two-dimensional flow, it can also be used for three-dimensional flows and analyses of such flows are currently in progress.

Our method is inspired by a theorem of Donoho[13] which states that the optimal way to denoise a signal f, sampled on N points and perturbed by an additive Gaussian white noise of variance $\langle n^2 \rangle$ (where $\langle \cdot \rangle$ denotes the average), is to take its orthonormal wavelet transform $\tilde{f}$, and then select only those coefficients with absolute value larger than the threshold $\epsilon_D = (2\langle n^2 \rangle \log N)^{1/2}$ before reconstructing the denoised signal $f_>$. In many cases (e.g., turbulent signals) it is not possible to guarantee *a priori* the Gaussianity of the noise and to know its variance $\langle n^2 \rangle$. Moreover, the statistical theory of homogeneous turbulence suggests that the noise may have some correlation, which corresponds to a scaling law steeper than for a white noise (i.e., $k^{-5/3}$ in three dimensions and k^{-3} in two dimensions). Therefore we propose the following algorithm (the wavelet decomposition and reconstruction is explained in Sec. II D):

(1) Decompose the signal f into orthonormal wavelet coefficients $\tilde{f}$.

(2) Select the coefficients larger than the threshold ϵ_T

$=(2\langle f^2\rangle\log N)^{1/2}$, where we overestimate the variance of the Gaussian noise we want to remove, by taking the variance $\langle f^2\rangle$ of the total signal instead of $\langle n^2\rangle$, therefore $\epsilon_T\gtrsim\epsilon_D$.

(3) Reconstruct the signal $f_>$ from the wavelet coefficients $|\tilde{f}|>\epsilon_T$.

(4) Reconstruct the signal $f_<$ from the wavelet coefficients $|\tilde{f}|\leq\epsilon_T$ and test Gaussianity by computing the odd moments $M_{m<}=\langle f_<^{2m+1}\rangle$, with $m=1$, 2 or 3, the skewness $S_<=\langle f_<^3\rangle/\langle f_<^2\rangle^{3/2}$, and the flatness $F_<=\langle f_<^4\rangle/\langle f_<^2\rangle^2$ of the signal $f_<$ reconstructed from the discarded coefficients $\tilde{f}_<$.

(5) If $M_{m<}\simeq0$, $S_<\simeq0$ and $F_<\simeq3$, $f_<$ is Gaussian and therefore the remaining part $f_>$ is the non-Gaussian denoised signal we wanted to extract.

(6) If $|S_<|>\varepsilon$ and $|F_<-3|>\varepsilon$, where ε is the prescribed precision of the algorithm, we do another iteration [starting in (2)] with the new threshold $\epsilon_{T'}=(2\langle f_<^2\rangle\log N)^{1/2}$, which is based on the variance $\langle f_<^2\rangle$ of the signal reconstructed from the discarded coefficients of the previous iteration. If further iterations are necessary, we use a new threshold $\epsilon_{T''}=\frac{1}{2}(\epsilon_T+\epsilon_{T'})$, intermediate between the previous ones, together with a classical bisection type algorithm.

The iterative process is stopped, either if the discarded coefficients are Gaussian, or if there are no Gaussian coefficients. In the second case all wavelet coefficients are retained, which means that there was no Gaussian noise present in the signal.

D. Application to two-dimensional turbulent flows

To extract coherent vortices in two-dimensional turbulent flows we take the vorticity field $\omega(x,y)$ as the signal to be denoised and apply the algorithm described above. We develop $\omega(x,y)$ as an orthogonal wavelet series from the largest scale $l_{\max}=2^0$ to the smallest scale $l_{\min}=2^{J-1}$ ($N=2^{2J}$) using a two-dimensional multiresolution analysis (MRA):[5,4]

$$\omega(x,y)=\bar{\omega}_{0,0,0}\phi_{0,0,0}(x,y)$$

$$+\sum_{j=0}^{J-1}\sum_{i_x=0}^{2^j-1}\sum_{i_y=0}^{2^j-1}\sum_{\mu=1}^{3}\tilde{\omega}_{j,i_x,i_y}^{\mu}\,\psi_{j,i_x,i_y}^{\mu}(x,y),\quad(1)$$

with $\phi_{j,i_x,i_y}(x,y)=\phi_{j,i_x}(x)\phi_{j,i_y}(y)$, and

$$\psi_{j,i_x,i_y}^{\mu}(x,y)=\{\psi_{j,i_x}(x)\phi_{j,i_y}(y)(\mu=1),$$

$$\phi_{j,i_x}(x)\psi_{j,i_y}(y)(\mu=2),\quad\psi_{j,i_x}(x)\psi_{j,i_y}(y)(\mu=3)\},\quad(2)$$

where $\phi_{j,i}$ and $\psi_{j,i}$ are the one-dimensional scaling function and the corresponding wavelet, respectively. Due to the orthogonality, the scaling coefficients are given by $\bar{\omega}_{0,0,0}=\langle\omega,\phi_{0,0,0}\rangle$ and the wavelet coefficients are given by $\tilde{\omega}_{j,i_x,i_y}^{\mu}=\langle\omega,\psi_{j,i_x,i_y}^{\mu}\rangle$, where $\langle\cdot,\cdot\rangle$ denotes the L^2-inner product.

Using the above algorithm, we split the vorticity field into $\omega_>(x,y)$ and $\omega_<(x,y)$ by applying the threshold $\epsilon_T=(2\langle\omega^2\rangle\log N)^{1/2}$, where $\langle\omega^2\rangle=\langle\omega,\omega\rangle=2Z$ with Z the total

enstrophy and N the number of grid points. The advantage of our method is that this threshold is objective and therefore has no adjustable parameters. The two fields thus obtained, $\omega_>$ and $\omega_<$, are orthogonal, which ensures a separation of the total enstrophy into $Z=Z_>+Z_<$ because the interaction term $\langle\omega_>,\omega_<\rangle$ is zero.

In Sec. III we propose a new method of computing turbulent flows which is based on the coherent vortex extraction algorithm we have just described.

III. COHERENT VORTEX SIMULATION (CVS)

A. Turbulent flow computation: Direct numerical simulation versus modeled numerical simulation

In contrast to the statistical theory and to most laboratory experiments, which deal with L^2-norm averaged quantities, numerical experiments deal with nonaveraged instantaneous quantities. We compute deterministically the evolution of one flow realization at a time, and perform the desired averages afterwards. There are two ways of computing turbulent flows: either by direct numerical simulation (DNS), or by modeled numerical simulation (MNS).

In DNS we compute all degrees of freedom of the flow, whose number N increases with the Reynolds number, as Re in two dimensions and as $Re^{9/4}$ in three dimensions. In this case both the nonlinear dynamics and the linear dissipation are fully resolved by computing the time evolution of these N degrees of freedom. Unfortunately, with present computers we cannot reach Reynolds numbers larger than a few thousand. Therefore, to compute fully developed turbulent flows $(Re>10^4)$ we are forced to use some form of MNS.

In MNS [e.g., unsteady Reynolds averaged (URANS), large eddy simulations (LES), or nonlinear Galerkin methods] one supposes that most of the modes can be discarded, provided that some term(s) or some new equations(s) are added to model the effect of the discarded modes [called unresolved modes and denoted $(\cdot)_<$] on the retained modes [called resolved modes and denoted $(\cdot)_>$]. Ideally, in order to reduce the computational cost as much as possible, the number of resolved modes $N_>$ should be much smaller than the number of unresolved modes $N_<$. Furthermore, $N_>$ should increase more slowly with Re than N does to be able to compute fully developed turbulent regimes, i.e., the large Re limit. We conjectured that this is the case for the wavelet representation in two dimensions, because the number $N_>$ of retained modes is roughly proportional to the number of vortices, which seems to increase more slowly with Re than N.[1] The $N_>$ resolved modes are then computed deterministically, while it is assumed that the $N_<$ unresolved modes are passive, namely that there is no nonlinear instability of some unresolved modes that can grow in such a way that they would deterministically affect the resolved modes. Therefore it must be ensured that the unresolved modes have reached a quasi-equilibrium state, characterized by a Gaussian PDF, and are sufficiently decorrelated. In this case it is no longer necessary to compute the evolution of the unresolved modes in detail because, if they are in Gaussian statistical equilibrium, they are characterized entirely by their mean and variance. The model describing the effect of the unresolved

modes onto the resolved modes can then be specified completely once the mean and variance of the unresolved modes can be parametrized as a function of the resolved modes.

We consider the incompressible two-dimensional Navier–Stokes equation in vorticity–velocity formulation,

$$\partial_t \omega + \boldsymbol{\nabla} \cdot (\omega \mathbf{V}) - \nu \nabla^2 \omega = \boldsymbol{\nabla} \times \mathbf{F}$$

$$\boldsymbol{\nabla} \cdot \mathbf{V} = 0, \tag{3}$$

with $\mathbf{F}$ a forcing term and

$$\mathbf{V} = \boldsymbol{\nabla}^\perp \nabla^{-2} \omega, \tag{4}$$

where $\boldsymbol{\nabla}^\perp = (-\partial_y, \partial_x)$, ∇^{-2} denotes the Green's function of the Laplacian, and ν is the kinematic viscosity. The above set of equations is completed by appropriate initial and boundary conditions.

Using the orthogonal wavelet decomposition we split the vorticity field into coherent and incoherent components,

$$\omega = \omega_> + \omega_< . \tag{5}$$

The corresponding velocity fields can be reconstructed using the Biot–Savart kernel (4):

$$\mathbf{V}_> = \boldsymbol{\nabla}^\perp \nabla^{-2} \omega_>$$

$$\mathbf{V}_< = \boldsymbol{\nabla}^\perp \nabla^{-2} \omega_< , \tag{6}$$

and it follows that

$$\mathbf{V} = \mathbf{V}_> + \mathbf{V}_< . \tag{7}$$

Since the wavelet decomposition is orthogonal, we have $\langle \omega^2 \rangle = \langle \omega_>^2 \rangle + \langle \omega_<^2 \rangle$. However, the decomposition of the velocity field is only approximately orthogonal, i.e., $\langle \mathbf{V}^2 \rangle = \langle \mathbf{V}_>^2 \rangle + \langle \mathbf{V}_<^2 \rangle + \varepsilon$ with $\varepsilon / \langle \mathbf{V}^2 \rangle \ll 1$ (cf. Table II). This is due to the fact that wavelets are almost eigenfunctions of Biot–Savart kernel, i.e., their localization in physical space and in Fourier space is well preserved. Note that for the Fourier decomposition $\varepsilon = 0$.

B. Principle of CVS

We now describe a new method, called coherent vortex simulation (CVS), to solve the deterministic evolution of the coherent vorticity $\omega_>$, while modeling statistically the effect of the incoherent vorticity $\omega_<$. This method is in the spirit of LES,[14] but in contrast to LES it uses a nonlinear filter that depends on each flow realization (using the wavelet thresholding procedure presented in Sec. II). The wavelet filter corresponds to an orthogonal projection, implying $(\omega_<)_> = 0$, and is hence idempotent, i.e., $(\omega_>)_> = \omega_>$, which is not the case for all LES filters (e.g., the Gaussian filter). We filter the two-dimensional Navier–Stokes equations (3) using the nonlinear wavelet filter and obtain the evolution equation for the coherent vorticity $\omega_>$:

$$\partial_t \omega_> + \boldsymbol{\nabla} \cdot (\omega \mathbf{V})_> - \nu \nabla^2 \omega_> = \boldsymbol{\nabla} \times \mathbf{F}_>$$

$$\boldsymbol{\nabla} \cdot \mathbf{V}_> = 0. \tag{8}$$

To model the effect of the discarded coefficients, which correspond to the incoherent stress, we propose (as in LES) to use a Boussinesq ansatz (cf. Sec. III D).

For the nonlinear term we use Leonard's triple decomposition,[14] because the nonlinear term is computed with the same adapted grid as the linear term (i.e., without dealiasing). Using (5) and (7) we decompose the nonlinear term of (8) into

$$(\omega \mathbf{V})_> = \omega_> \mathbf{V}_> + L + C + R, \tag{9}$$

where

$$L = (\omega_> \mathbf{V}_>)_> - \omega_> \mathbf{V}_> ,$$

$$C = (\omega_< \mathbf{V}_>)_> + (\omega_> \mathbf{V}_<)_> ,$$

$$R = (\omega_< \mathbf{V}_<)_> ,$$

denoting the Leonard stress L, the cross stress C, and the Reynolds stress R, respectively. The sum of these unknown terms corresponds to the incoherent stress:

$$\tau = (\omega \mathbf{V})_> - \omega_> \mathbf{V}_> = L + C + R, \tag{10}$$

which describes the effect of the discarded incoherent terms on the resolved coherent terms. Note that, due to the localization property of the wavelet representation, the Leonard stress L is actually negligible because $(\omega_> \mathbf{V}_>)_> \simeq \omega_> \mathbf{V}_>$.[15]

The filtered Navier–Stokes equations (8) can be rewritten as:

$$\partial_t \omega_> + \boldsymbol{\nabla} \cdot (\omega_> \mathbf{V}_>) - \nu \nabla^2 \omega_> = \boldsymbol{\nabla} \times \mathbf{F}_> - \boldsymbol{\nabla} \cdot \tau$$

$$\boldsymbol{\nabla} \cdot \mathbf{V}_> = 0. \tag{11}$$

A detailed analysis of the nonlinear term $\boldsymbol{\nabla} \cdot (\omega_> \mathbf{V}_>)$ decomposed into wavelet space is provided in Sec. IV F.

C. DNS using CVS

If with the CVS method we consider a very small threshold, there is no longer any need to model the effect of the incoherent part because the incoherent stress is then negligible, and in this case CVS becomes DNS. Note that even when the wavelet threshold tends to zero, the number of discarded incoherent modes may still be large (cf. Fig. 9 and Sec. IV H), due to the excellent compression properties of wavelets for turbulent flows. This is reflected in the fact that many wavelet coefficients are essentially zero and can therefore be discarded without losing a significant amount of enstrophy (cf. Sec. IV H).

To obtain the coherent variables $\omega_>$ and $\mathbf{V}_>$ we deterministically integrate (11) with $\tau = 0$, since the variables are non-Gaussian and correspond to a dynamical system out of statistical equilibrium. We propose to solve these equations in an adaptive wavelet basis.[15–17] The separation into coherent and incoherent components is performed at each time step. The adaptive wavelet basis retains only those wavelet modes corresponding to the coherent vortices and it is remapped at each time step in order to follow their motions, in both space and scale. In fact, this numerical scheme combines the advantages of both the Eulerian representation (because it projects the solution onto an orthonormal basis) and the Lagrangian representation (because it follows the coherent vortices by adapting the basis at each time step).

TABLE I. Comparison of the statistical properties of L^2-norm quantities using Fourier low pass filtering ($k_c = 11 \text{ m}^{-1}$) and wavelet thresholding ($\epsilon_T = (2\langle \omega^2 \rangle \log N)^{1/2} = 13.75 \text{ s}^{-1}$).

	Fourier		Wavelet	
# of coefficients N	65536	(100%)	65 536	(100%)
$N_>$	484	(0.7%)	458	(0.7%)
$N_<$	65052	(99.3%)	65 078	(99.3%)
Energy $E = \frac{1}{2}\int |\mathbf{V}|^2 \, dx$	0.591	(100%)	0.591	(100%)
$E_>$	0.588	(99.4%)	0.586	(99.2%)
$E_<$	3.3×10^{-3}	(0.6%)	2.6×10^{-3}	(0.4%)
Enstrophy $Z = \frac{1}{2}\int |\omega|^2 \, dx$	9.82	(100%)	9.82	(100%)
$Z_>$	8.92	(90.8%)	9.26	(94.3%)
$Z_<$	0.90	(9.2%)	0.56	(5.7%)
Palinstrophy $P = \frac{1}{2}\int |\nabla \omega|^2 \, dx$	725	(100%)	725	(100%)
$P_>$	261	(36%)	404	(55%)
$P_<$	464	(64%)	360	(49%)

D. MNS using CVS

Up to now no modeling has been done, and Eq. (11) is not closed as long as τ depends on the incoherent unresolved terms. To close it we propose two possibilities.

(1) A Boussinesq ansatz as for the LES method,[14] which assumes that τ is proportional to the negative gradient of the coherent vorticity: $\tau = -\nu_T \nabla \omega_>$ with ν_T a turbulent viscosity coefficient. The turbulent viscosity ν_T can be estimated, either using Smagorinsky's model,[14] or taking ν_T proportional to the enstrophy fluxes in wavelet space, such that, where enstrophy flows from large to small scales, ν_T is positive, and, where enstrophy flows from small to large scales (i.e., backscatter), ν_T becomes negative. This second method for estimating the turbulent viscosity is in the spirit of Germano's dynamical procedure used for LES.[14]

(2) τ can otherwise be modeled as a Gaussian stochastic forcing term, proportional to the variances $\langle \omega_<^2 \rangle$ and $\langle V_<^2 \rangle$ computed at the previous time steps (the means $\langle \omega_< \rangle = \langle V_< \rangle = 0$). This modeling is made possible since the time evolution of the incoherent background, characterized by the time scale $t_< = (Z_<)^{-1/2}$, is much slower than the characteristic time scale $t_> = (Z_>)^{-1/2}$ of the coherent vortex motions, because $Z_> \gg Z_<$ (cf. Table I). This behavior of the incoherent background had already been noticed, and discussed in comparison to Fourier filtering in Refs. 10 and 15.

The CVS method relies on the assumption that the incoherent part of the flow remains Gaussian, which is true as long as the nonlinear interactions between the incoherent modes remains weak. This assumption is valid in regions where the density of coherent vortices is sufficient, because the strain they exert on the incoherent background flow then inhibits the development of any nonlinearity there.[1] However, there may be regions, although of small spatial support, where the density of coherent vortices is not sufficient to control the incoherent nonlinear term. In this case, there are two solutions.

(1) To locally refine the wavelet basis in these regions in order to deterministically compute the effect of the incoherent nonlinear term (no longer neglected), which will lead to the formation of new coherent vortices by nonlinear instability of the incoherent background flow.

(2) To directly model the formation of new coherent vortices by adding locally to the wavelet coefficients the amount of coherent enstrophy which should be transferred from the incoherent enstrophy by nonlinear instability. This procedure is similar to the wavelet forcing proposed by Schneider and Farge.[18]

IV. RESULTS

In this section we present the separation into coherent and incoherent components applied to a two-dimensional homogeneous turbulent flow. We then show the analysis of the nonlinear terms of the two-dimensional Navier–Stokes equations for the coherent and incoherent contributions. Finally, to illustrate our approach we use the CVS method to compute a two-dimensional mixing layer.

A. Turbulent flow to be analyzed

We consider a two-dimensional homogeneous isotropic turbulent flow, forced at wave number $k_I = 4 \text{ m}^{-1}$, considering the same parameters as the simulation of Legras et al.[19] We compute its evolution by DNS using a fully dealiased pseudospectral code with Newtonian dissipation. The resolution is $N = 256^2$, which corresponds to a Reynolds number of 1000. The flow has reached a statistically steady state characterized by the fact that the energy spectrum no longer changes. We analyze one flow realization chosen at time $t = 75 \text{ s}$ (which corresponds to 17 eddy-turnover times). In principle, when the flow is statistically steady, all flow realizations are equivalent (in the classical statistical sense based on L^2-norm quantities, such as the energy spectrum) and we would obtain the same statistical results with any other realization. We decompose this vorticity field into coherent and incoherent components, using the algorithm presented in the previous paragraph with Battle–Lemarié spline wavelets of order 6 (cf. Fig. 1). We then compare these results with those obtained using a classical decomposition of vorticity, into low wave number modes (i.e., large eddies as used for LES) and high wave number modes (i.e., small eddies), before reconstructing the vorticity field from these two components. In both cases, using either the wavelet decomposition or the Fourier decomposition, the compression ratio is the same: the number of modes retained [i.e., coherent or low wave number modes denoted $(\cdot)_>$] represents 0.7% of the total number of modes N.

B. Vorticity compression

We apply our wavelet segmentation algorithm (cf. Sec. II C) to split the vorticity field ω into coherent components $\omega_>$ and incoherent components $\omega_<$. The coherent flow can be reconstructed from only 0.7% of the total number of wavelet modes N, equivalent to a compression ratio of $N/N_> = 143$. Table II shows that these few ($N_> = 0.7\%$ of N) coherent modes retain most of the energy ($E_> = 99.2\%$ of $E = \frac{1}{2}\int |\mathbf{V}|^2 \, dx$) and most of the enstrophy ($Z_> = 94.3\%$ of $Z = \frac{1}{2}\int |\omega|^2 \, dx$). About half of the palinstrophy ($P_> = 55\%$ of $P = \frac{1}{2}\int |\nabla \omega|^2 \, dx$) is due to the mu-
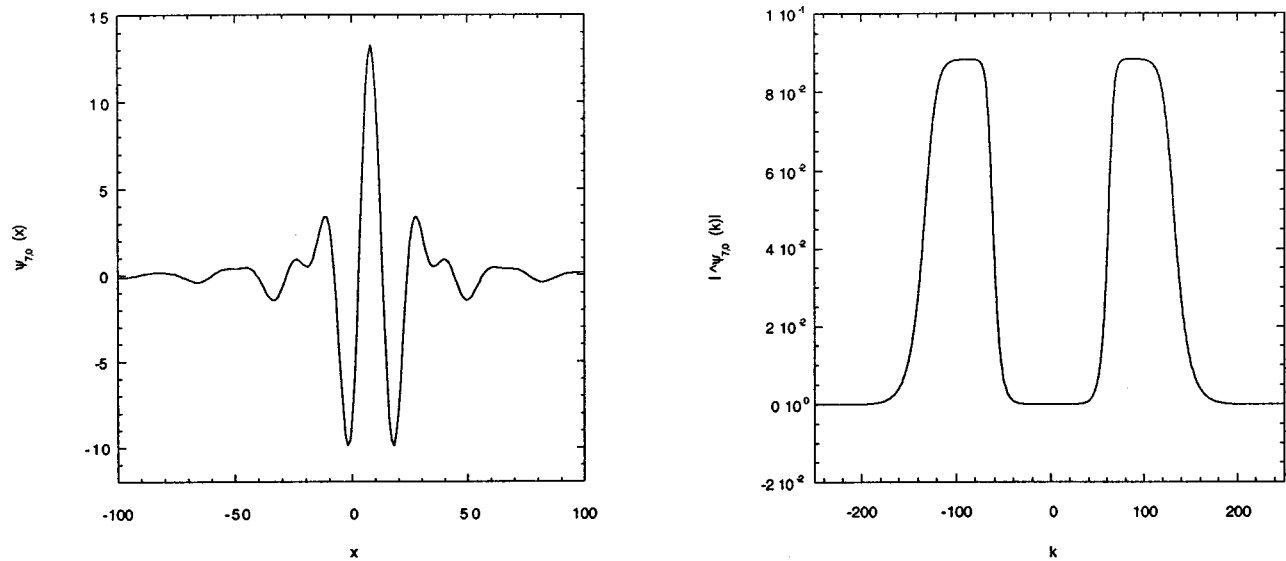
FIG. 1. Quintic spline wavelet $\psi_{j,i}(x)$ for scale $j=7$ and position $i=0$ in physical space (left) and in Fourier space (right).

tual straining of coherent vortices, while the rest corresponds to the stretching of the vorticity filaments in the background.

We then compare (cf. Table I) the compression obtained by wavelet thresholding with the compression obtained using a linear Fourier filtering, as used in LES. Note that it is not possible to retain exactly the same number of resolved modes due to the fact that the two-dimensional Fourier decomposition is done by tensor product of two one-dimensional decompositions, therefore $N_>$ should be a square number in this case. We decided to retain a few more Fourier modes than wavelet modes ($22^2 = 484$ vs 458), which gives a slight advantage to the Fourier filtering. Despite this, the Fourier compression retains less enstrophy (90.8% of Z) and palinstrophy (only 36% of P) than wavelet compression (94.3% of Z and 55% of P).

C. Coherent vortex extraction

Our algorithm is based on the sole assumption that there should be some (maybe only a few) components of the flow which correspond to a Gaussian probability distribution. We have checked that the algorithm's performance does not depend on the choice of the wavelet, as long as the wavelet has enough smoothness and vanishing moments, as is the case

for the spline wavelet of order 6 we have chosen (cf. Fig. 1). Now we verify *a posteriori* that the retained strong wavelet coefficients actually correspond to the coherent vortices. We observe that the spatial distributions of both vorticity [Fig. 2(a)] and velocity [Fig. 2(b)] reconstructed from these strong wavelet coefficients are very well preserved. The coherent fields have the same inhomogeneity as the original fields and exhibit very similar structures. On the contrary, the incoherent fields are homogeneous; moreover the incoherent velocity induced by the incoherent vorticity distribution is essentially zero. The coherent streamfunction is exactly the same as the total streamfunction, therefore the incoherent streamfunction is almost zero [cf. Fig. 2(c)].

The pointwise correlations between vorticity ω and streamfunction Ψ, which is a discrete version of the coherence function $\omega = F(\Psi)$, are almost identical for both the total flow and the coherent flow [cf. Fig. 2(d)]. Both the coherent and total flows have the same scatter plots corresponding to a superposition of coherent vortices, each vortex being characterized by a function F. The same scatter plot for the background flow (i.e., from the vorticity $\omega_<$ and stream function $\Psi_<$ reconstructed from the weakest wavelet coefficients) does not show any correlation, which confirms

TABLE II. Statistical properties of the statistically stationary vorticity field at $t=75$ s using wavelet thresholding ($\epsilon_T = (2\langle\omega^2\rangle \log N)^{1/2} = 13.75$ s^{-1}).

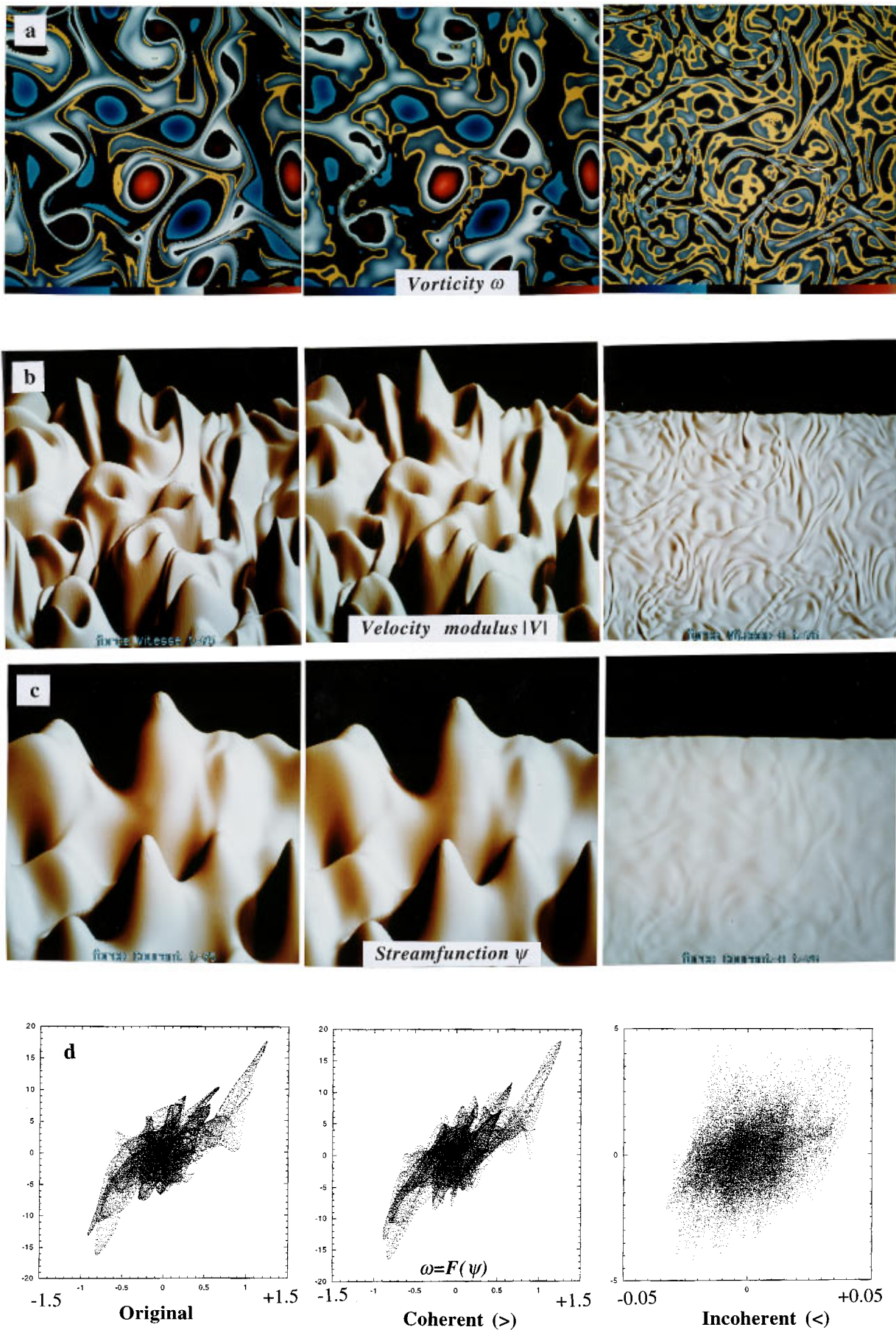| Quantity	Definition	ω total	$\omega_>$ coherent	$\omega_<$ incoherent
# of coefficients	N	65 536	458	65078
% of coefficients		100%	0.7%	99.3%
Second moment (variance)	$M_2 = \langle\omega^2\rangle = (1/N)\Sigma_{i=1}^N \omega_i^2$	20	19	1
Third moment	$M_3 = (1/N)\Sigma_{i=1}^N \omega_i^3$	8	8	0
Fourth moment	$M_4 = (1/N)\Sigma_{i=1}^N \omega_i^4$	1 736	1 659	4
Fifth moment	$M_5 = (1/N)\Sigma_{i=1}^N \omega_i^5$	1 903	2 911	0
Sixth moment	$M_6 = (1/N)\Sigma_{i=1}^N \omega_i^6$	282 763	276 378	28
Skewness	$S = M_3/M_2^{3/2}$	0	0	0
Flatness	$F = M_4/M_2^2$	5	5	3

FIG. 2. Wavelet filtering of vorticity. Left: total field. Middle: coherent part. Right: incoherent part. (a) Vorticity ω. (b) Modulus of velocity $|\mathbf{V}|$. (c) Stream function Ψ. (d) Coherence scatter plot ω vs Ψ.
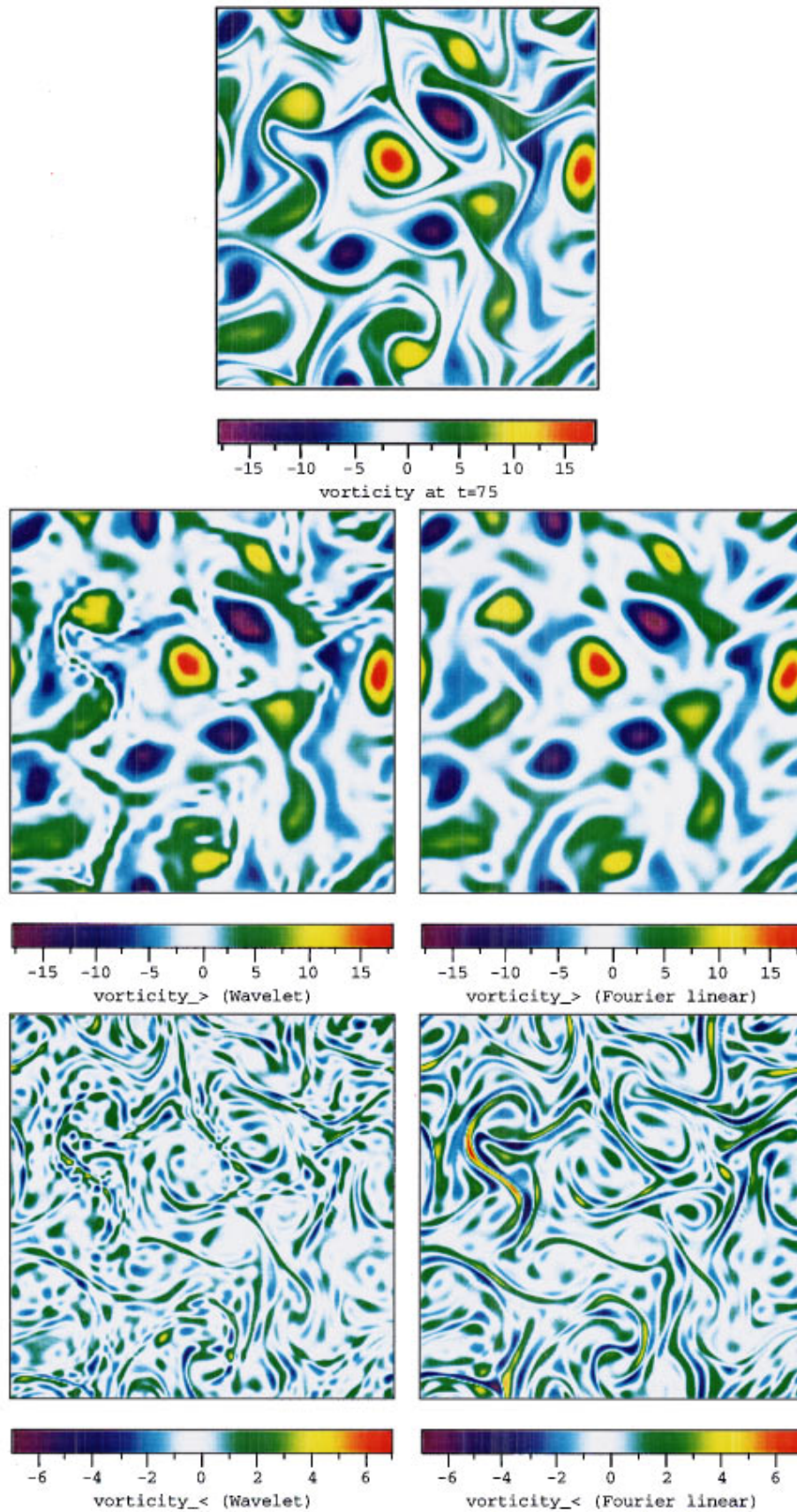
FIG. 3. Comparison of nonlinear wavelet filtering (left) with linear Fourier filtering (right) of vorticity for the same compression rate $N/N_> = 143$. Top: total vorticity ω. Middle: resolved part $\omega_>$. Bottom: unresolved part $\omega_<$.

2196   Phys. Fluids, Vol. 11, No. 8, August 1999

Farge, Schneider, and Kevlahan
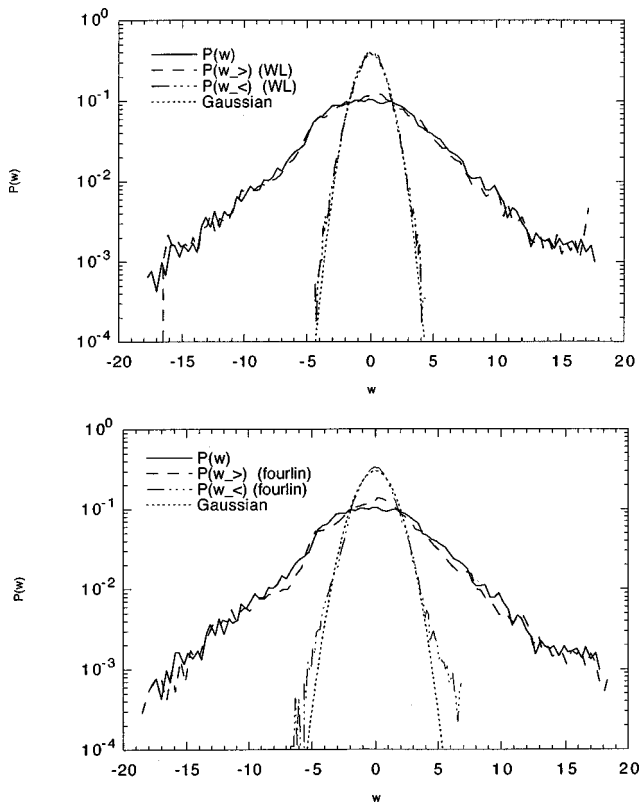
FIG. 4. PDF of vorticity. Top: nonlinear wavelet filtering. Bottom: linear Fourier filtering. The solid lines correspond to the total vorticity ω, the dashed lines to the coherent part $\omega_>$, the dotted-dashed lines to the incoherent part $\omega_<$, and the dotted lines to a Gaussian fit.

TABLE III. Comparison of the statistical properties of the nonlinear term and its components using Fourier low pass filtering ($k_c = 11$ m^{-1}) and wavelet thresholding ($\epsilon_T = (2\langle\omega^2\rangle\log N)^{1/2} = 13.75$ s^{-1}).

Quantity	Fourier		Wavelet	
# of coefficients $N_>$	484	(0.7%)	458	(0.7%)
# of coefficients $N_<$	65 052	(99.3%)	65078	(99.3%)
	L^2-norm	Flatness	L^2-norm	Flatness
ω	4.4	4	4.4	4
$\omega_>$	4.2	5	4.3	5
$\omega_<$	1.3	4	1.1	3
u	0.8	3	0.8	3
$u_>$	0.7	3	0.7	3
$u_<$	0.1	4	0.1	3
v	0.8	3	0.8	3
$v_>$	0.8	3	0.8	3
$v_<$	0.1	5	0.05	3
$\partial_x\omega$	27.0	6	27.0	6
$\partial_x\omega_>$	16.2	4	20.2	5
$\partial_x\omega_<$	21.4	9	18.7	6
$\partial_y\omega$	27.0	8	27.0	8
$\partial_y\omega_>$	16.1	3	20.0	5
$\partial_y\omega_<$	21.6	10	19.2	8
$v\cdot\nabla\omega$	12.1	9	12.1	9
$v_>\cdot\nabla\omega_>$	7.8	5	11.9	12
$v_<\cdot\nabla\omega_<$	0.9	26	0.9	13
$v_>\cdot\nabla\omega_<$	11.2	9	12.0	12
$v_<\cdot\nabla\omega_>$	1.0	10	1.4	11

that the background flow is incoherent and contains no coherent vortices. Note that the scatter plot of the incoherent components has been rescaled and actually corresponds to a very small cloud of points located at the center of the scatter plot of the original fields.

If we perform the separation using Fourier filtering (with the same compression rate $N/N_> = 143$), we observe that the vorticity field $(\omega_>)^f$ reconstructed from the large scales is smoother than the vorticity field $(\omega_>)^w$ reconstructed from the strong wavelet coefficients (cf. Fig. 3). We also ascertain that the incoherent field $\omega_<$ is more homogeneous and smoother for the wavelet filtering than for the Fourier filtering, because $(\omega_<)^f$ presents localized strong gradient regions.

D. Vorticity PDF

In Table II we verify *a posteriori* that the incoherent components are Gaussian with skewness $S_<^w \simeq 0$, flatness $F_<^w \simeq 3$ and odd moments $M_{3<}^w \cong M_{5<}^w \simeq 0$. The superscript $(\cdot)^w$ denotes the wavelet filtering, while the superscript $(\cdot)^f$ denotes the Fourier filtering. In contrast to the incoherent components, the coherent components have non-Gaussian statistics essentially identical to those of the total vorticity, with $S_>^w = S = 0.1$, $F_>^w = F = 5$, and $M_{n>}^w \simeq M_n$. This is also illustrated at the top of Fig. 4 where we have superimposed the three PDFs, for the total vorticity ω, the coherent vorticity $\omega_>$, and the incoherent vorticity $\omega_<$. The

PDF of the incoherent vorticity has a parabolic shape similar to the PDF of a Gaussian distribution plotted in log–lin coordinates. When we compare on Fig. 4 (bottom) these results with those obtained with the Fourier decomposition, we observe that the PDF of the high wave number modes is not perfectly Gaussian and has a flatness 4, while flatness is 3 for the wavelet filtering (cf. Table III).

Using the Biot–Savart kernel (4) we reconstruct the three velocity fields $\mathbf{V}$, $\mathbf{V}_>^w$, and $\mathbf{V}_<^w$, induced by the three corresponding vorticity fields. The coherent velocity $\mathbf{V}_>^w = (u,v)_>^w$ has the same Gaussian PDF as the total velocity $\mathbf{V} = (u,v)$, and the incoherent velocity $\mathbf{V}_<^w = (u,v)_<^w$ has a Gaussian PDF with a much smaller variance (cf. Table III).

The vorticity and velocity PDFs of the high wave number Fourier modes are not Gaussian, with flatness 4 for $u_<$ and $\omega_<$, and flatness 5 for $v_<$ (cf. Table III and Fig. 4—bottom). This may have important implications for LES, because in this method the high wave number modes are not computed but instead modeled statistically assuming that they are quasi-Gaussian.

E. Energy spectrum

In Fig. 5 we compare the energy spectra associated with the coherent and incoherent components of the wavelet filtering with the energy spectra associated with the low wave number and high wave number modes of the Fourier filtering. It has been shown that, when using wavelet filtering, both coherent and incoherent components are multiscale,[10]
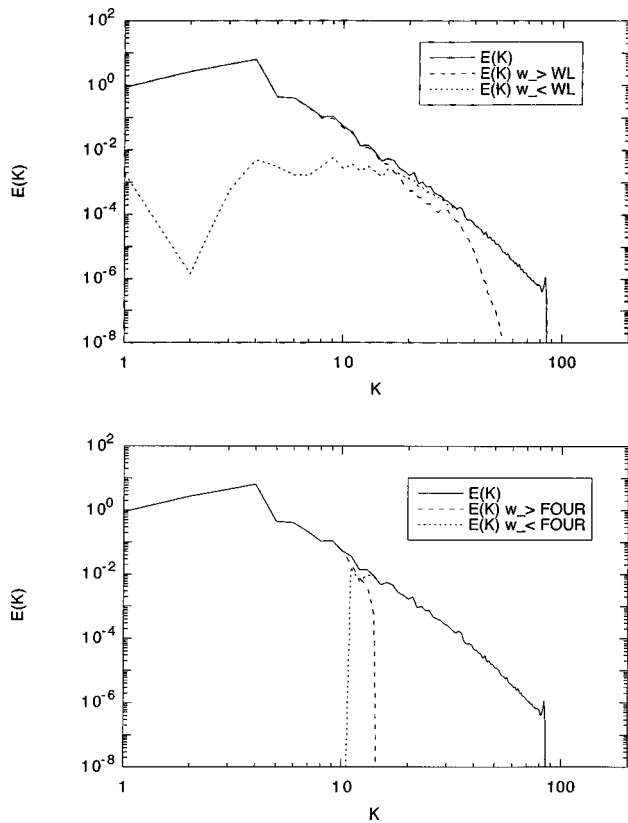
FIG. 5. Energy spectrum $E(k)$. Top: nonlinear wavelet filtering. Bottom: linear Fourier filtering. The solid lines correspond to the total field $\mathbf{V}$, the dashed lines to the resolved part $\mathbf{V}_>$, and the dotted lines to the unresolved part $\mathbf{V}_<$.

although the coherent part dominates at low wave numbers and the incoherent part dominates at high wave numbers (Fig. 5—top). This behavior comes from the fact that the energy spectrum is the Fourier transform of the two-point correlation and is less sensitive to localized events at small scales. In fact, the energy spectrum (as all other L^2-norm statistical quantities) is poorly adapted to study intermittent flow fields.[7] In particular, the small scales associated with the coherent vortices have a spatial support too small to be well-detected by the two-point correlation; this explains why the incoherent component, which is homogeneous and therefore tends to be dense in space, dominates at high wave numbers.

F. Nonlinear term

At the top of Fig. 6 we have plotted the nonlinear term $\nabla \cdot (\omega \mathbf{V}) = \mathbf{V} \cdot \nabla \omega$ together with its PDF (cf. Fig. 7—top), which is highly non-Gaussian. The fact that the PDF of the nonlinear term is non-Gaussian is not surprising since Gaussianity is stable under linear operations but not under multiplication. The nonlinear term of the Navier–Stokes equation is responsible for the cascade mechanism and for the resulting non-Gaussianity of turbulent fields. Since this term is difficult to solve, it is essential for the performance of the computational scheme that the resolved modes $\mathbf{V}_> \cdot \nabla \omega_>$ retain as much of it as possible. This property is illustrated in Fig. 7, which shows that the PDF of the nonlinear term computed from the coherent wavelet modes is essentially the same as the PDF of the total nonlinear term, which is not true for the Fourier filtering. This difference is confirmed by plotting the components of the nonlinear term split into $\mathbf{V} \cdot \nabla \omega = \mathbf{V}_> \cdot \nabla \omega_> + \mathbf{V}_> \cdot \nabla \omega_< + \mathbf{V}_< \cdot \nabla \omega_> + \mathbf{V}_< \cdot \nabla \omega_<$ for both Fourier and wavelet filterings (cf. Fig. 6 and Table III).

First, we observe that for both Fourier and wavelet filterings the cross term $\mathbf{V}_< \cdot \nabla \omega_>$ and the Reynolds term $\mathbf{V}_< \cdot \nabla \omega_<$ are negligible (less than 10% of $\|\mathbf{V} \cdot \nabla \omega\|_2$, cf. Table III). But the Reynolds term $\mathbf{V}_< \cdot \nabla \omega_<$ is more non-Gaussian, with flatness 26, for Fourier filtering than for wavelet filtering, with flatness 13 (cf. Fig. 6 and Table III).

In Fig. 6 we compare the two other terms $\mathbf{V}_> \cdot \nabla \omega_>$ and $\mathbf{V}_> \cdot \nabla \omega_<$. They are similar (in amplitude and regularity) for the wavelet filtering, while the term $\mathbf{V}_> \cdot \nabla \omega_>$ is smaller (cf. Table III) and smoother than the term $\mathbf{V}_> \cdot \nabla \omega_<$ for the Fourier filtering.

In summary, the Fourier filtering tends to have the resolved term $(\mathbf{V}_> \cdot \nabla \omega_>)^F$ smoother and more Gaussian than the unfiltered nonlinear term $\mathbf{V} \cdot \nabla \omega$. The wavelet filtering has the opposite behavior: the resolved nonlinear term $(\mathbf{V}_> \cdot \nabla \omega_>)^\omega$ retains the pronounced gradients and is more non-Gaussian than the unfiltered nonlinear term $\mathbf{V} \cdot \nabla \omega$, while the unresolved term $(\mathbf{V}_< \cdot \nabla \omega_<)^\omega$ is more Gaussian than with Fourier filtering. This is an advantage of the wavelet filtering, because it is important that the resolved nonlinearity, which is deterministically computed, should be less Gaussian, while the unresolved nonlinearity, whose effect is statistically modeled, should be more Gaussian.

G. Vorticity gradients

In Fig. 8 we have plotted the PDF of the vorticity gradients in the x direction (gradients in the y direction are similar and are therefore omitted) in order to understand the discrepancy we have observed in the behavior of the nonlinear term depending on the segmentation we operate. As before, we find that the PDF of vorticity gradients, computed from the coherent wavelet modes, are very similar to the PDF of the vorticity gradients of the original flow, but this is not the case for the Fourier filtering, because the tails (extreme events) of the original flow PDF have been lost. This is also illustrated by considering the L^2 norm of the vorticity gradients (i.e., palinstrophy P), which is weaker for the retained Fourier modes than for the discarded Fourier modes (cf. Tables I and III). Ideally one would like the opposite to be true, in order to guarantee the performance of the LES method. This is in fact the case for the wavelet filtering where the retained vorticity gradients are stronger than the discarded vorticity gradients (cf. Tables III). The difference is due to the space-scale adaptivity of the wavelet method which allows a much more accurate representation of the strong gradients, while the global cutoff scale of the Fourier filter destroys the strong gradients necessary to compute the nonlinear term. Moreover, for the Fourier filtering the vorticity gradients of the retained modes are quasi-Gaussian with flatness 4, while the vorticity gradients of the discarded modes are non-Gaussian with flatness 9 (cf. Tables III), although the reverse would be desirable.
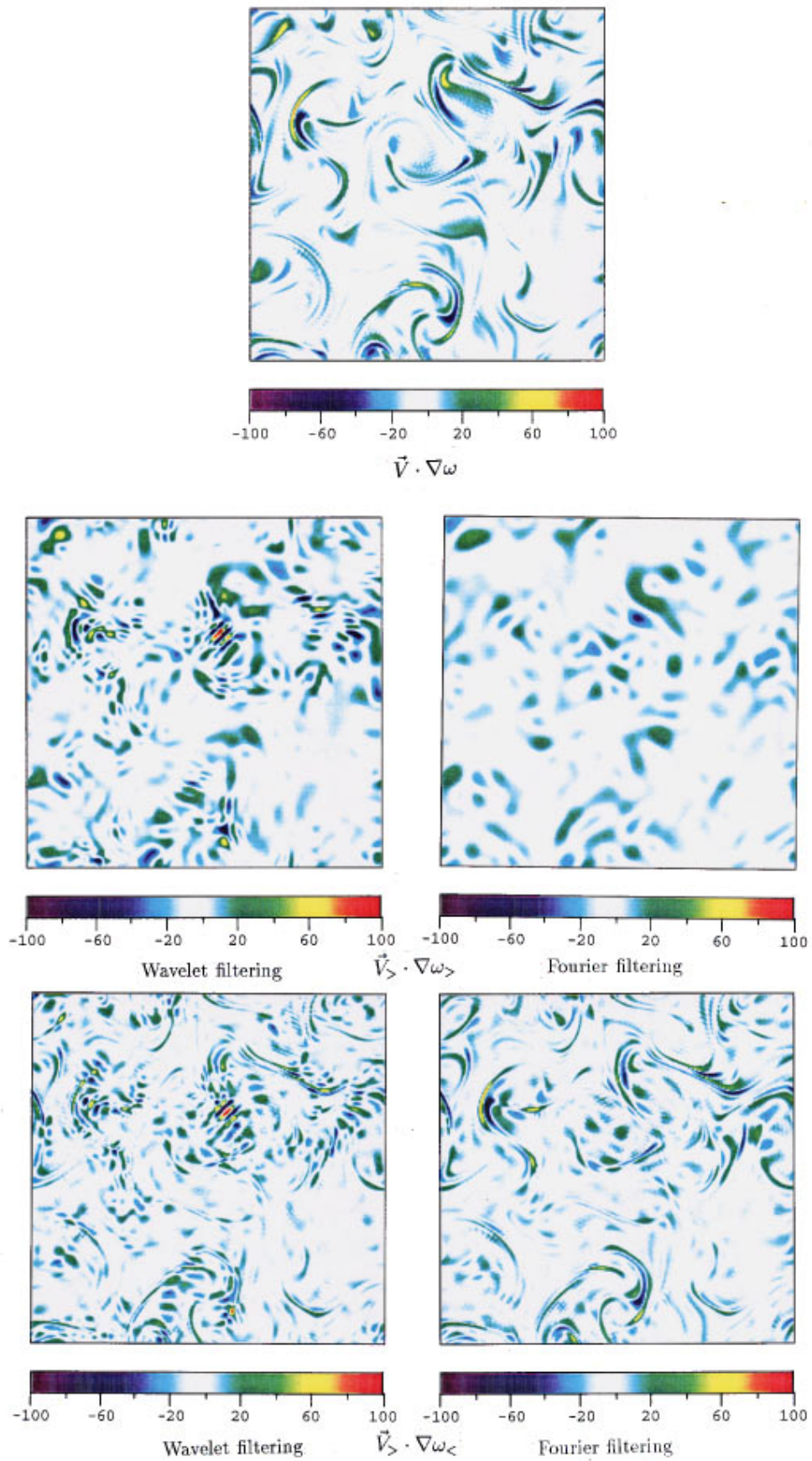
FIG. 6. Comparison of nonlinear wavelet filtering (left) with linear Fourier filtering (right) of the nonlinear term $\mathbf{V}\cdot\nabla\omega$ for the same compression rate $N/N_> = 143$. Top: total term. Middle: $\mathbf{V}_>\cdot\nabla\omega_>$. Bottom: $\mathbf{V}_>\cdot\nabla\omega_<$.

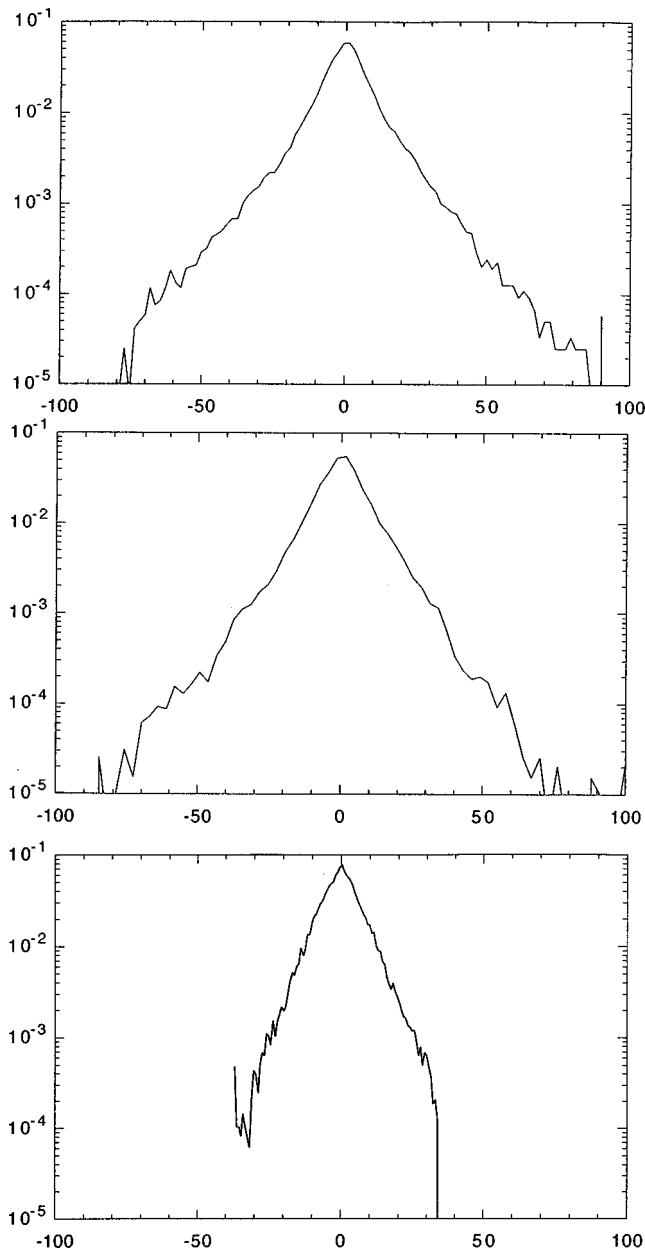FIG. 7. PDF of the nonlinear term $\mathbf{V} \cdot D\omega$. Top: total term. Middle: non-linear wavelet filtering $(\mathbf{V}_> \cdot D\omega_>)^\omega$. Bottom: linear Fourier filtering $(\mathbf{V}_> \cdot D\omega_>)^F$.
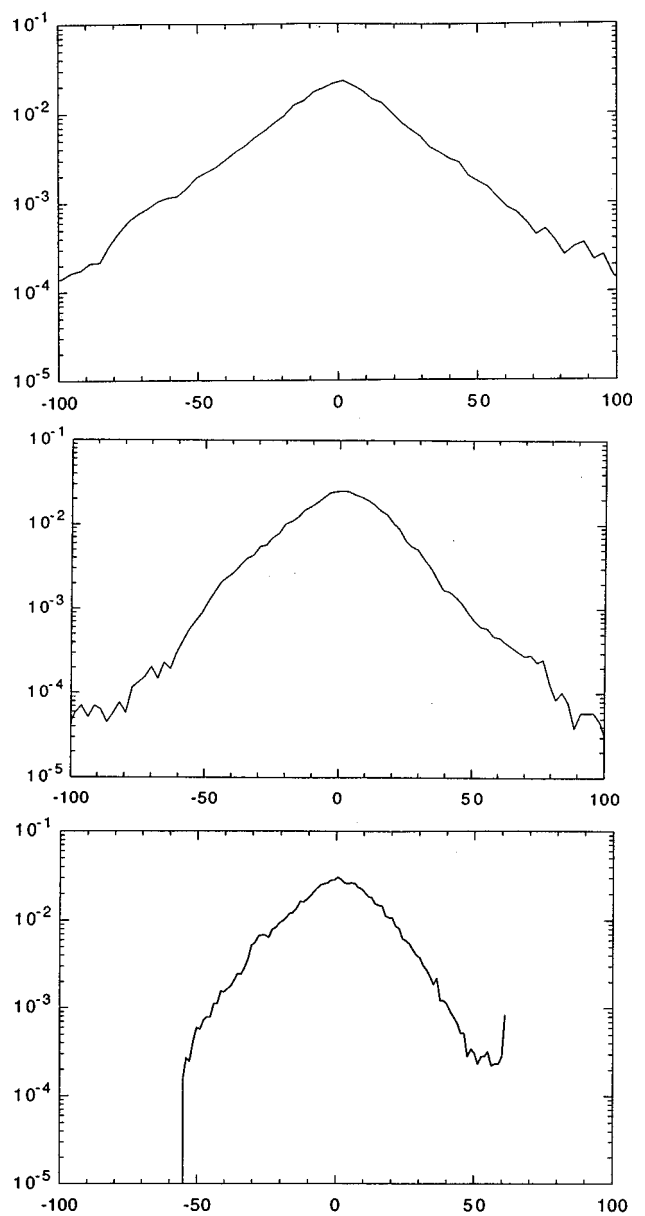
FIG. 8. PDF of the vorticity gradient $\partial_x \omega$ ($\partial_y \omega$ behaves similarly). Top: total term. Middle: nonlinear wavelet filtering $(\partial_x \omega)^\omega$. Bottom: linear Fourier filtering $(\partial_x \omega)^F$.

H. Application of CVS

We now use the CVS method to compute the evolution of a temporally developing mixing layer. We take as initial condition a hyperbolic-tangent velocity profile, which is known to be inviscidly unstable. We superimpose in the vortical region a Gaussian white noise to trigger the Kelvin–Helmholtz instability. For more details on the numerical simulation we refer the reader to Ref. 20. The integration is done by computing only the evolution of the coherent part $(\omega_>, \mathbf{V}_>)$, while discarding the incoherent part $(\omega_<, \mathbf{V}_<)$ at each time step, which corresponds to Eq. (11). This is a DNS since we choose a very small threshold, $\epsilon = c \epsilon_T$ with $c = 10^{-3}$, because we do not model the effect of the incoherent modes on the coherent modes in taking $\tau = 0$.

In Fig. 9 we show the coherent vorticity field $\omega_>$ at time $t = 37.5$ s (i.e., nine eddy turnover times), the corresponding wavelet coefficients $\tilde{\omega}_>$ used for the computation, and the associated refined grid in physical space. The time evolution of the coherent vorticity and the energy spectrum are similar to the evolution of the total vorticity[20] and of the total energy spectrum (cf. Fig. 9) computed using a classical pseudospectral method at resolution 256^2. As soon as the vortices are formed by Kelvin–Helmholtz instability (around $t = 7$ s), the number of retained wavelet coefficients remains quasiconstant for the rest of the simulation. The retained wavelet coefficients represent only 8% of the total number of coefficients necessary for a pseudospectral integration. To obtain a higher compression, a turbulence model with $\tau \neq 0$ (cf. Sec. III D) is necessary to parametrize the effect of the discarded
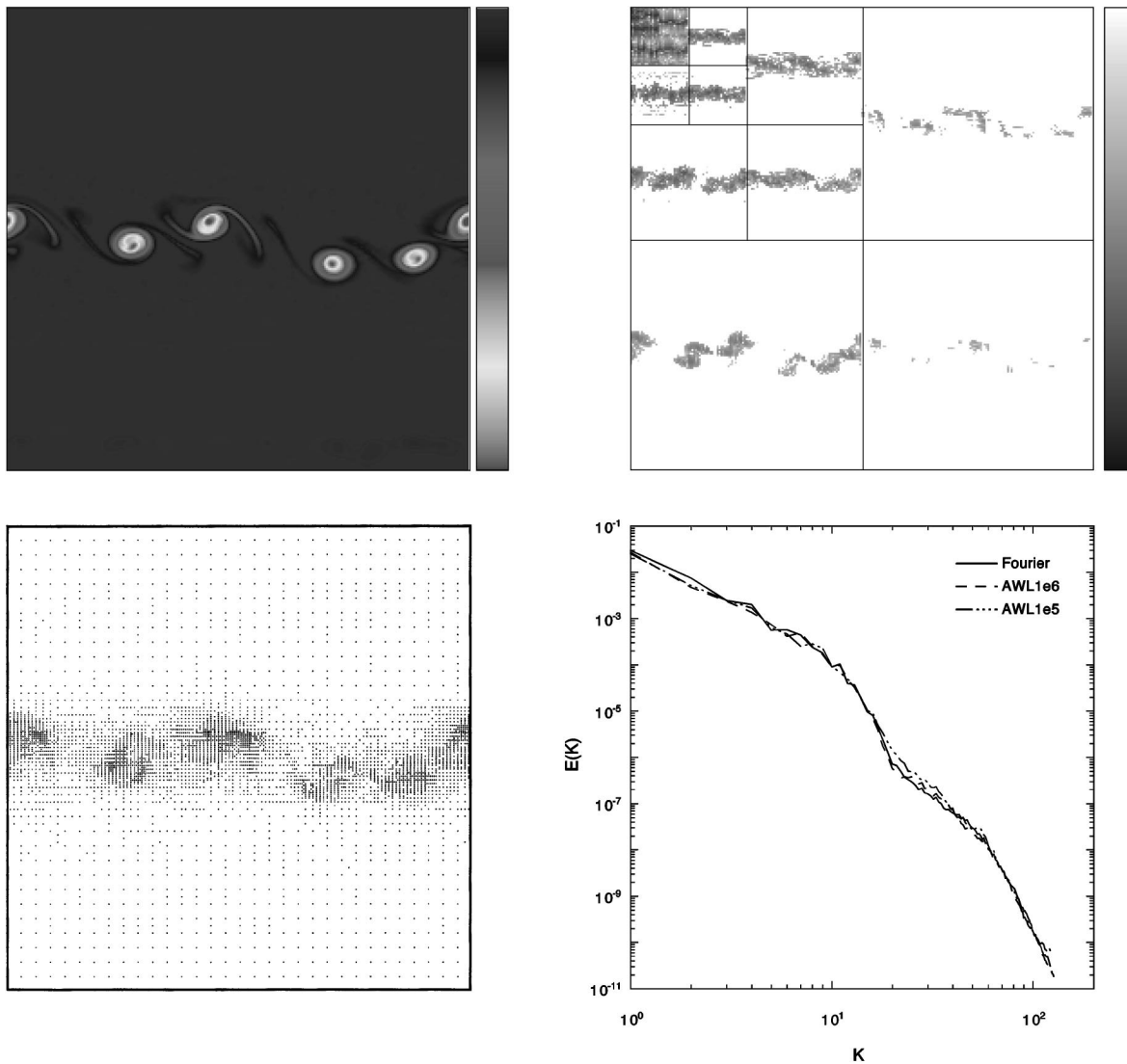
FIG. 9. Mixing layer computed with CVS in an adaptive wavelet basis. Top left: vorticity field at $t=37.5$ s. Top right: corresponding coherent wavelet coefficients at $t=37.5$ s. Note that only 8% of the 256^2 wavelet coefficients represent the coherent part of the flow and are used in the computation. The wavelet coefficients (gray entries) are plotted using a logarithmic scale. The coefficients $\tilde{\omega}^{\mu}_{j,i_x,i_y}$ are placed at $x=2^j(1-\delta_{\mu,1})+i_x$, $y=2^j(1-\delta_{\mu,2})+i_y$, δ being the Kronecker tensor, with the origin in the upper left corner and the y-coordinate oriented downwards. The largest scales correspond to the smallest square (top left). The smallest scales correspond to the largest squares (bottom left for the horizontal direction, top right for the vertical direction and bottom right for the diagonal direction). Bottom left: corresponding adaptive grid in physical space at $t=37.5$ s). Note that it dynamically adapts to the flow evolution in space and scale. Bottom right: corresponding energy spectrum at $t=37.5$ s. We compare the same mixing layer computed with a Fourier pseudo-spectral code (solid line) or with the CVS (dotted line for $\epsilon=10^{-5}$ and dashed line for $\epsilon=10^{-6}$).

coefficients, which then contain a non-negligible amount of enstrophy.

V. CONCLUSION

In this paper we have introduced and validated a wavelet-based algorithm for separating the Gaussian and non-Gaussian parts of a turbulent flow. This algorithm leads to a new definition of the coherent vortices: they are the components of the flow that contribute to the non-Gaussian part of the vorticity PDF. The algorithm is applied to a two-dimensional homogeneous turbulent flow and we show that the Gaussian and non-Gaussian parts of the vorticity field can be well separated using the nonlinear wavelet filtering we have proposed. It is also proven that the non-Gaussian

part of vorticity corresponds to the coherent vortices, i.e., compact regions of strong vorticity and vorticity gradients characterized by a local correlation between vorticity and stream function. Furthermore, it turns out that the coherent vortices can be represented by only a few modes (less than 0.7% of the total for a resolution 256^2), while the Gaussian incoherent field makes up the rest. Note that larger compressions are obtained at higher resolutions.

We have proposed a new method based on this vortex extraction algorithm for calculating two-dimensional turbulent flows. This method, called coherent vortex simulation (CVS), is described in detail and is applied to compute a mixing layer. We discuss some of its potential advantages with respect to classical methods (e.g., LES). Perhaps the most interesting aspect of this approach is that the separation

involves no adjustable parameters and guarantees the Gaussianity of the discarded modes, which allows the statistical methods (that have been developed based on the assumption of Gaussian statistics) to be used only for that part of the flow where they are actually valid. Since the background flow is homogeneous and Gaussian, the classical theory of homogeneous turbulence is valid there, which is not the case for the coherent vortex flow, which is non-Gaussian and inhomogeneous. The CVS method is not restricted to the two-dimensional case and can be extended to compute three-dimensional turbulent flows. It is based on deterministically computing the coherent vortex flow using an adaptive wavelet basis, and modeling statistically the incoherent background flow. We believe that CVS combines statistical and deterministic approaches in a simple and natural way.

[1] N. K.-R. Kevlahan and M. Farge, ''Vorticity filaments in two-dimensional turbulence: Creation, stability and effect,'' J. Fluid Mech. **346**, 49 (1997).

[2] A. Grossmann and J. Morlet, ''Decomposition of Hardy functions into square integrable wavelets of constant shape,'' SIAM J. Math. Anal. **15**, 723 (1984).

[3] M. Farge and G. Rabreau, ''Transformée en ondelettes pour détecter et analyser les structures cohérentes dans les écoulements turbulents bidimensionnels,'' C. R. Acad. Sci. Paris Sér. IIb **307**, 433 (1988).

[4] M. Farge, ''Wavelet transforms and their applications to turbulence,'' Annu. Rev. Fluid Mech. **24**, 395 (1992).

[5] I. Daubechies, *Ten Lectures on Wavelets* (SIAM, Philadelphia, 1992).

[6] M. Farge, Y. Guezennec, C. M. Ho, and C. Meneveau, ''Continuous wavelet analysis of coherent structures,'' CTR Proc. Summer Program 737 (1990).

[7] K. Schneider, M. Farge, and N. K.-R. Kevlahan, ''Wavelet approach to study intermittency in turbulence,'' Preprint ICT, Universität Karlsruhe (TH) (1999).

[8] C. Meneveau, ''Analysis of turbulence in the orthonormal wavelet representation,'' J. Fluid Mech. **232**, 469 (1991).

[9] M. Farge and M. Holschneider, ''Interpretation of two-dimensional turbulence spectrum in terms of singularity in the vortex cores,'' Europhys. Lett. **15**, 737 (1990).

[10] M. Farge and T. Philipovitch, ''Coherent structure analysis and extraction using wavelets,'' in *Progress in Wavelet Analysis and Applications*, edited by Y. Meyer and S. Roques (Editions Frontières, Gif-sur-Yvette, 1993), 477.

[11] M. Farge, E. Goirand, Y. Meyer, F. Pascal, and M. V. Wickerhauser, ''Improved predictability of two-dimensional turbulent flows using wavelet packet compression,'' Fluid Dyn. Res. **10**, 229 (1992).

[12] M. V. Wickerhauser, M. Farge, E. Goirand, E. Wesfreid, and E. Cubillo, ''Efficiency comparison of wavelet packet and adapted local cosine bases for compression of a two-dimensional turbulent flow,'' in *Wavelets: Theory, Algorithms and Applications*, edited by C. K. Chui *et al.* (Academic Press, San Diego, 1994), p. 509.

[13] D. Donoho, ''Unconditional bases are optimal bases for data compression and statistical estimation,'' Appl. Comput. Harmon. Anal. **1**, 100 (1993).

[14] J. H. Ferziger, ''Large Eddy Simulation,'' *Simulation and Modeling of Turbulent Flows*, edited by T. B. Gatski, M. Y. Hussaini, and J. L. Lumley, ICASE Series in Computational Science and Engineering 109, New York (1996).

[15] K. Schneider and M. Farge, ''Wavelet approach for modeling and computing turbulence,'' *Advances in Turbulence Modeling*, von Karman Institute for Fluid Dynamics Lecture Series 1998-05, Bruxelles (1998).

[16] J. Fröhlich and K. Schneider, ''An adaptive wavelet-vaguelette algorithm for the solution of PDEs,'' J. Comput. Phys. **130**, 174 (1997).

[17] K. Schneider, N. K.-R. Kevlahan, and M. Farge, ''Comparison of an adaptive wavelet method and nonlinearly filtered pseudospectral methods for two-dimensional turbulence,'' Theor. Comput. Fluid Dyn. **9**, 191 (1997).

[18] K. Schneider and M. Farge, ''Wavelet forcing for numerical simulation of two-dimensional turbulence,'' C. R. Acad. Sci. Paris, Sér. IIb: **325**, 263 (1997).

[19] B. Legras, P. Santangelo, and R. Benzi, ''High resolution numerical experiments for forced two-dimensional turbulence,'' Europhys. Lett. **5**, 37 (1988).

[20] K. Schneider and M. Farge, ''Numerical simulation of a temporally growing mixing layer in an adaptive wavelet basis,'' submitted to C. R. Acad. Sci. Paris, Sér. IIb (1999).